INTERNATIONAL ATOMIC ENERGY AGENCY
UNITED NATIONS EDUCATIONAL, SCIENTIFIC AND CULTURAL ORGANIZATION
INTERNATIONAL CENTRE FOR THEORETICAL PHYSICS
I.C.T.P., P.O. BOX 586, 34100 TRIESTE, ITALY, CABLE: CENTRATOM TRIESTE

SMR/534-21

ICTP/WMO WORKSHOP ON EXTRA-TROPICAL AND TROPICAL LIMITED AREA MODELLING
22 October - 3 November 1990

"Vertical Coordinates"

Z.I. JANJIC
University of Belgrade
Department of Meteorology
Belgrade, Yugoslavia

Please note: These are preliminary notes intended for internal distribution only.

Vertical coordinates

- Phillips (1957),

$$\sigma = (p - p_T)/(p_S - p_T),$$

terrain-following, no problem with the lower boundary condition, most popular.

- Early problem, non-cancellation of errors in the two terms of PGF (Smagorinsky et al., 1967). Many ideas about, see e.g. review by Mesinger and Janjić (1985).

- Currently used schemes result of three-step procedure: (i) calculation of geopotential at terrain following coordinate surfaces, (ii) linear extrapolation/interpolation to constant pressure surfaces, and (iii) evaluation of the pressure gradient force on the constant pressure surfaces.

- Importance of a "coherency", or "hydrostatic consistency" in steps (i) and (ii) stressed by Rousseau and Pham (1971), Janjić (1977, 1979).

- Let the horizontal domain be scaled in such a way that the grid distance be equal to 1. Due to periodicity, for any function f(i), where i is the horizontal index, f(M+i)=f(i). The values of M and L_m are 120 and 15, respectively.

- Consider spectral horizontal representation in terms of trigonometric functions which is equivalent to the grid-point representation on the M-point grid. The term "equivalent" is used here to denote the requirement that the spectral representation have the same number of degrees of freedom as the grid-point representation, and yield the same values at the grid points of the M-point grid. This requirement will be satisfied if the coefficients of the truncated trigonometric series are computed using the approximate Fourier transform formulae.

- In order to calculate the error, spectrally represented temperatures on the σ levels are needed. Following e.g. Mesinger and Janjić (1987), the temperatures are retrieved from the geopotential.

- Problems with consistency, even if required explicitely, for steep slopes of sigma surfaces and/or thin sigma layers (Mesinger, 1982; Mesinger and Janjić, 1985).

- Explicit vertical interpolation to constant pressure probably best (Mahrer 1984; Smagorinsky et al. 1967; Kurihara 1968, Miyakoda, 1973; Tomine and Abe 1982). Second order interpolation, energy conserving scheme by Mihailović and Janjić (1986).

- Problems with lateral diffusion, advection ...

- Higher and steeper mountains with higher resolution, more problems to be expected.

- Pressure? Problems with lower boundary, abandoned at U.K. Met Office (e.g., Cullen, 1985).

- z? Technical difficulties, no special benefit.

- θ? Technical difficulties, similar problems with PGF on sloping coordinate surfaces.

• Step-mountain η (Mesinger 1984)? Almost as simple as σ, quasi-horizontal coordinate surfaces, easy to implement in an existing sigma model, no difficulties with topography of any height or slope. Internal boundaries, conservational properties, vectorization - Mesinger et al. 1988, physical package - Janjić 1990.

Pressure Gradient Force Error in σ-coordinate Spectral Models (Janjić 1989)

• PGF errors in σ-coordinate spectral models often believed to be small or unimportant, little evidence published to support such a view (Simmons 1987; Simmons and Jiabian 1990).

• Consider horizontally homogenous atmosphere at rest, and in hydrostatic equilibrium. The pressure gradient force is zero everywhere, and the computed pressure gradient force in a discretized system will represent the error of the discretization method.

• Let the following information about this atmosphere be available in a vertical cross section along a constant latitude:

(i) Surface pressure p_S ($\ln p_S$) on equidistant horizontal grid with M independent points;

(ii) Surface geopotential Φ_S on the same M-point horizontal grid; and,

(iii) Geopotential Φ on the same M-point horizontal grid, and on L_m equidistant σ levels.

- For this purpose we choose the Bourke (1974) hydrostatic equation

$$\Phi_L = \Phi_{L+1} + R[(T_{L+1} + T_L)/2] \ln(\sigma_{L+1}/\sigma_L),$$
$$\text{for } L < L;$$
$$\Phi_{Lm} = \Phi_s + R\{T_{Lm} + [(T_{Lm} - T_{Lm-1})/\ln(\sigma_{Lm}/\sigma_{Lm-1})] \times \ln(1/\sigma_{Lm})/2\} \times \ln(1/\sigma_{Lm}).$$

- The spectrally represented temperatures can be obtained from the geopotentials using either of the following procedures:
(i) Grid point values of temperature are computed from the grid point values of geopotential, and then the temperature is converted into the spectral form; or
(ii) The geopotential is converted into the spectral form, and then the spectrally represented temperatures are obtained from the original, spectral form of Bourke's (1974) hydrostatic equation. Due to linearity of the operators involved, both procedures yield the same answer.

Having defined the temperatures, the pressure gradient force error of the spectral method is calculated using the following procedure:

- The spectral coefficients of $\partial \ln p_s/\partial x$ are calculated, and then these coefficients are used to recalculate the grid-point values of $\partial \ln p_s/\partial x$ on a regular 2M-point grid, i.e. the grid with twice the resolution of the original M-point grid.

- The spectral coefficients of $-\partial\Phi/\partial x$ are calculated from the spectrally represented geopotentials on each σ level, and then, the coefficients of the expansion of $-\partial\Phi/\partial x$ are used to compute the grid-point values of $-\partial\Phi/\partial x$ on the M-point grid. This is the first term of the pressure gradient force.

- The spectral coefficients of temperature on each σ level are used to recalculate the temperatures at the grid points of the 2M-point grid.

• The product $-RT\partial \ln p_s/\partial x$ is calculated at the grid points of the 2M-point grid on each σ level. Then, the spectral coefficients of this product are calculated, but all spectral components which cannot be represented on the M-point grid are truncated in order to avoid aliasing. The remaining coefficients are used to recalculate the values of $-RT\partial \ln p_s/\partial x$ at the grid points of the M-point grid. This is the second term of the pressure gradient force.

• The sum of the first and the second term of the pressure gradient force is the pressure gradient force error at the grid points of the M-point grid.

• The pressure gradient force error of the finite-difference method is calculated by the formula:

$$-\delta_x \Phi_\sigma - R\,\overline{T}^x\,\delta_x \ln p_s$$

• The geopotential on the σ levels from an analytical temperature profile T(p) (Mesinger 1982).

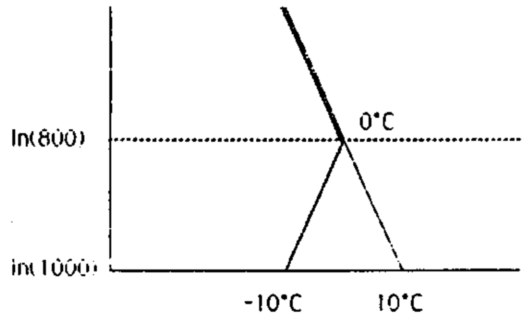

• In the main experiment, a single-grid-point mountain located in the middle of the domain, i.e. at the point with the horizontal index M/2+1. The remaining part of the domain is assumed to be flat. The surface pressure is 800 mb at the top of the mountain, and 1000 mb over the flat terrain (e.g. Mesinger and Janjić, 1987).

• In order to examine possible impact of the horizontal scale and shape of the mountain, the experiments are repeated with three different shapes of the three-point mountain: a triangular mountain with the slopes linear in lnp, an obelisk-shaped mountain, and a trapezoidal mountain (three-point elevated plateau).

• The surface pressures at the tops of the three-point mountains are again 800 mb. In the case of the obelisk-shaped mountain, the surface pressures at the two mountain points other than the top point are

$$p_s = [1000 - 200 \exp(-.25)] \text{ mb} = 844.24 \text{ mb}.$$

• The widths at the bases of the single-point, and the three-point mountains are 6° and 12°, respectively. The heights and slopes of the mountains are modest compared to the examples given e.g. by Mesinger and Collins (1987).

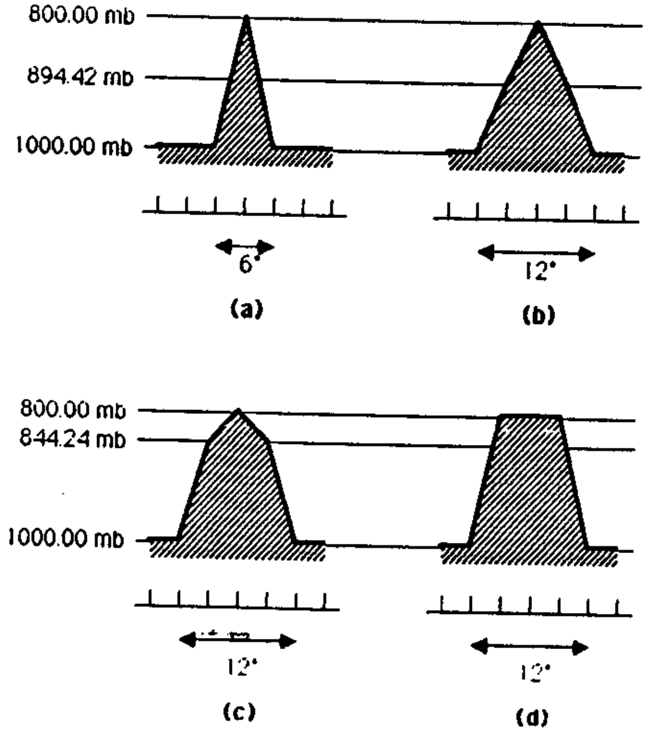

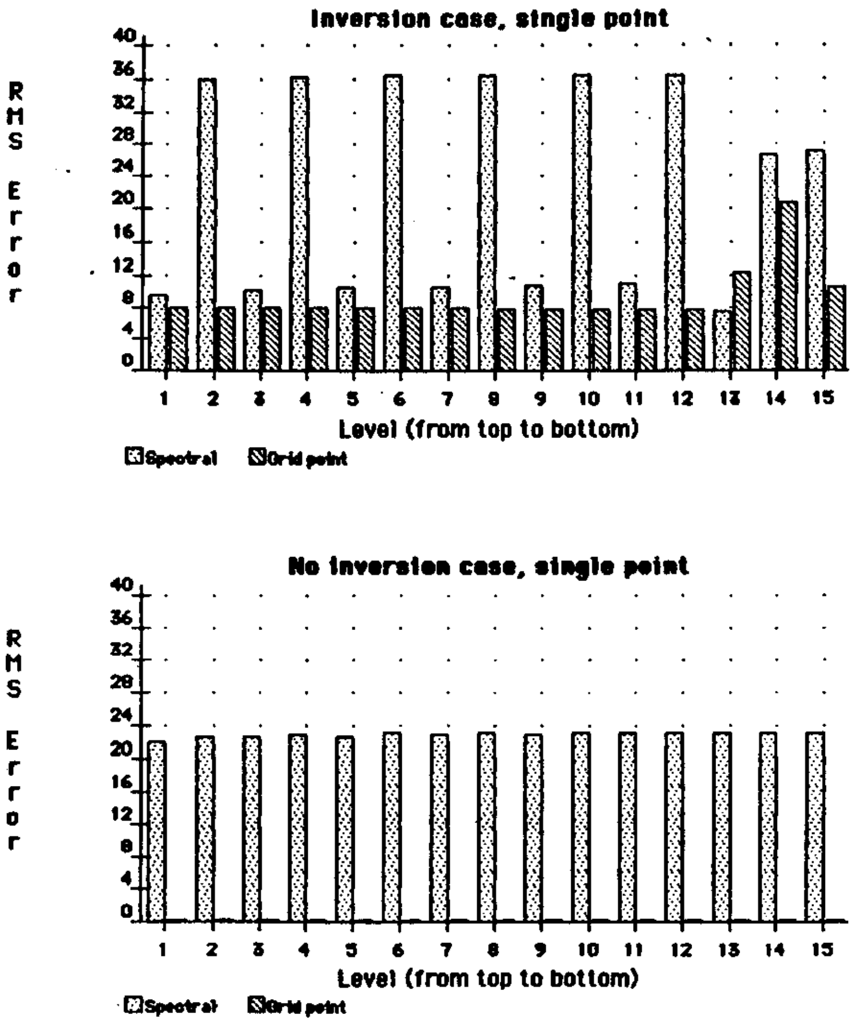

FIG. 3. The rms pressure gradient force errors corresponding to the single-grid point mountain for the inversion (upper panel) and no-inversion (lower panel) cases. The errors of the spectral and the finite-difference methods are represented by lightly shaded and cross-hatched bars, respectively. The plotted values are in units of geopotential.

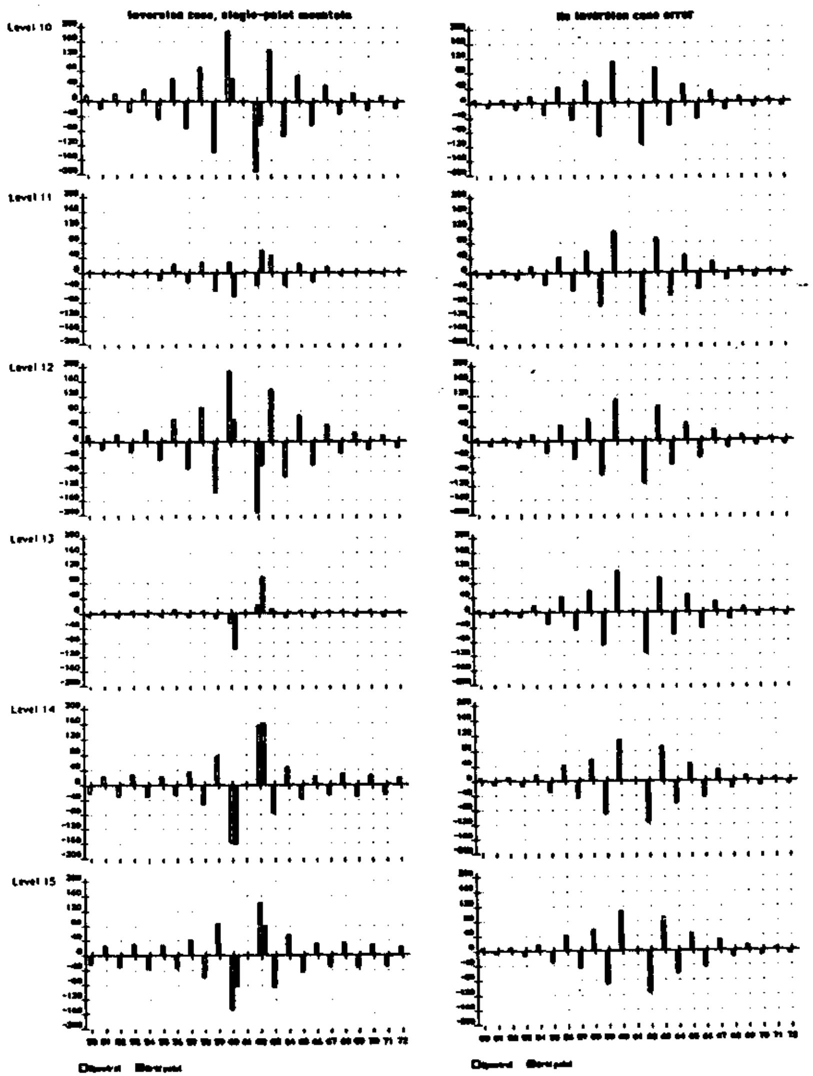

FIG. 4. Pressure gradient force error pattern around the mountain point at six lowest model levels for the spectral method (lightly shaded bars) and the finite-difference error (cross-hatched bars) for the inversion (left panel) and the no-inversion (right panel) cases. The finite-difference error bars are shifted for half a grid distance in the direction away from the mountain from the actual error locations. The ploted values are in units of geopotential.

than those of the finite-difference method, particularly in the no-inversion case; in this case, due to the temperature profile and the pressure gradient force scheme chosen, the errors of the finite-difference method are hardly detectable (cf. e.g. Mesinger and Janjić 1985).

In order to examine their spatial distribution, the pressure gradient force errors of the spectral method around the mountain point are plotted for the six lowest model levels in Fig. 4 (lightly shaded bars) for both inversion (left panel) and no-inversion (right panel) cases. Going further up, the error patterns of levels 11 and 10 very much repeat themselves, switching from one to the other, depending on whether the vertical index is even or odd. For comparison, the finite-difference pressure gradient force error is also displayed (cross-hatched bars) at the two points adjacent to the mountain point. It should be noted that the finite-difference errors are actually defined in between the mountain point and the two adjacent points. Thus, in the figure, they are shifted for half a grid distance away from their actual location.

Note that in the inversion case the amplitude of the spectral error wave packet is generally of the same order of magnitude as the errors of the finite-difference method. The large error of the spectral technique in the no-inversion case is somewhat surprising.

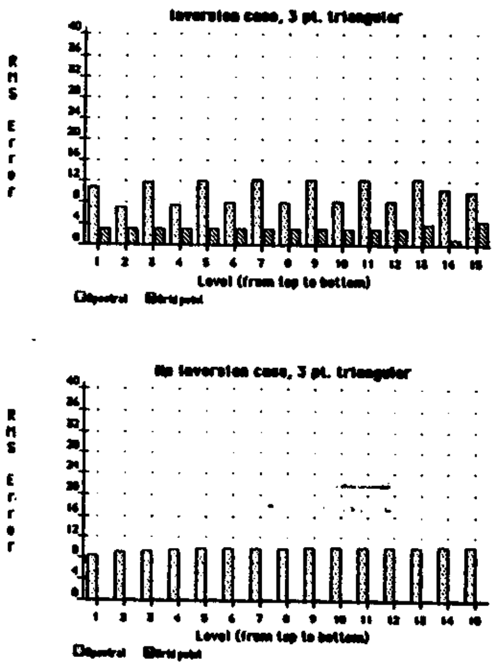

FIG. 5. Same as Fig. 3, but for the triangular three-point mountain.

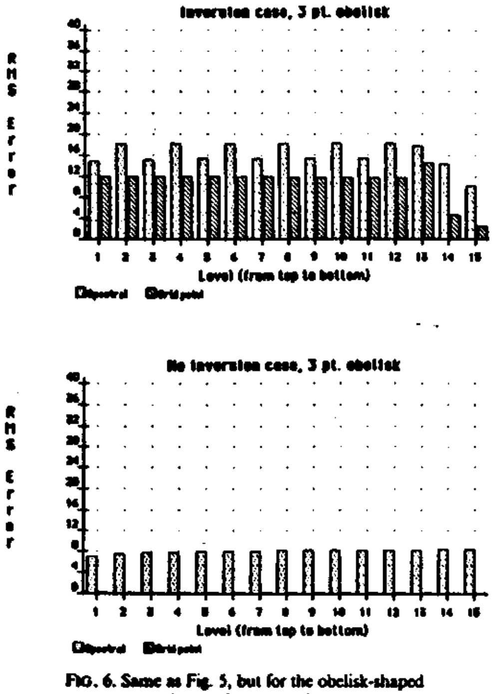

FIG. 6. Same as Fig. 5, but for the obelisk-shaped three-point mountain.

b. Three-point mountains

The rms pressure gradient force errors on the σ levels for the triangular, obelisk and trapezoidal shaped three-point mountains are shown in Figs. 5, 6 and 7, respectively. Again, the upper panels correspond to the inversion, and the lower ones to the no inversion cases. As before, the lightly shaded bars are reserved for the spectral, and the cross hatched bars for the finite-difference method.

As can be seen from Fig. 5, in the case of the triangular mountain, the rms errors are significantly reduced compared to the single-point mountain. However, in the rms sense, the pressure gradient force errors of the spectral method are again considerably larger. As expected, the errors of the finite-difference method in the no-inversion case are negligible.

Compared to the triangular mountain, the results for the obelisk-shaped mountain show a general increase of the rms errors in the inversion case. Note that the errors of the finite-difference method at higher levels are larger than those corresponding to the single-point mountain, and approach the errors of the spectral method. In the no-inversion case, the errors of the spectral method are slightly smaller than in the case of the triangular mountain.

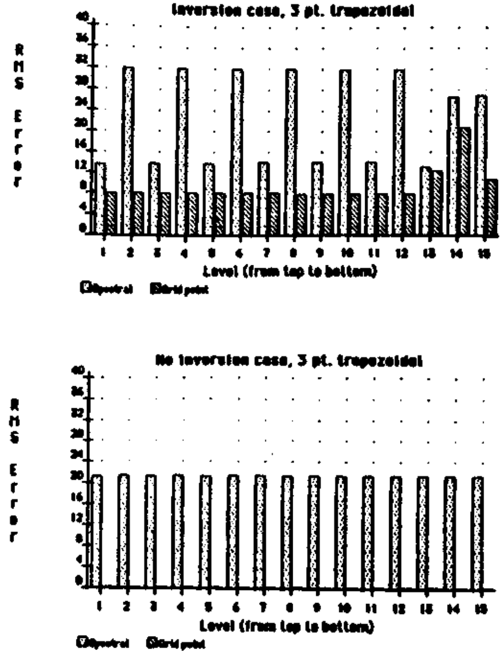

FIG. 7. Same as Fig. 6, but for the trapezoidal (elevated plateau) three-point mountain.

The errors for the trapezoidal mountain very much resemble those for the single-point mountain, except for the fact that the amplitude of two-grid-interval wave in the spectral rms error is now reduced.

In all tests with the three-point mountains, in the inversion case the amplitude of the spectral error wave packet (not shown) remained generally of the same order of magnitude as the errors of the finite-difference method.

4. Conclusions

The examples of small-scale mountains considered indicated that the σ-coordinate pressure gradient force errors of the spectral method can be large, and that the errors spread away from the mountains. In the rms sense, these errors were larger than the errors of the finite-difference method. In the inversion case, the amplitudes of the spectral error wave packets were generally of the same order of magnitude as the errors of the finite-difference method.

Contrary to the situation with the finite-difference method, the magnitude of the rms pressure gradient sensitivity to the absence of the inversion. Namely, error of the latter remained relatively large, while error of the former almost vanished.

The experiments with varying the horizontal s and the shape of the mountain showed the sensiti of the spectral method to the steepness of the mount Generally, the steeper the mountain, the larger pressure gradient force error. However, in the no version case, the rms errors of the generally ste obelisk mountain were slightly smaller than thos the triangular mountain.

The pressure gradient force errors of the spec method showed little sensitivity to changing from single-point mountain to the trapezoidal three-p mountain. Note that the steepnesses of the slope these two mountains are the same. This suggests the errors are less sensitive to the horizontal scal the mountain than to its steepness.

Relatively large pressure gradient force errors of spectral method observed in the no-inversion case dicate that the mechanisms responsible for the e are different from those of the finite-difference σ ordinate models. Consequently, the methods for ducing the error in the finite-difference models (Gary 1973; Janjić 1977, 1980; Mesinger and Ja 1985; Mihailović and Janjić 1986) should not be pected to operate effectively.

As already pointed out, it seems natural to ex difficulties with spectral representation in the prese of small-scale topography because of slow converge of the Fourier series. In this situation, in order to culate the pressure gradient force in σ-coordinate s tral models, it may be advantageous to use the fi difference technique on the finer grid used to elimi aliasing.

Acknowledgments. This research was supporte the Science Association of Serbia, Belgrade. The au is grateful to one of the reviewers for a suggestion lead to the definition of the three-point obelisk-sha mountain.

REFERENCES

Black, T. L., and Z. I. Janjić, 1988: Preliminary forecast results a step-mountain eta coordinate regional model. *Eighth Co ence on Numerical Weather Prediction,* Baltimore, Amer. teor. Soc., 442–447.
Bourke, W., 1974: A multi-level spectral model. I. Formulation hemispheric integrations. *Mon. Wea. Rev.,* 102, 687–701.
Gary, J. M., 1973: Estimate of truncation error in transforme ordinate, primitive equation atmospheric models. *J. Atmos.* 30, 223–233.
Janjić, Z. I., 1977: Pressure gradient force and advection sch used for forecasting with steep and small scale topography. *Phys. Atmos.,* 50, 186–199.
——, 1980: Numerical problems related to steep mountains in s coordinates. *Workshop on Mountains and Numerical We*

Tijana Janjić 1990, Oxon Hill High School Science Fair

5-Point Mountain

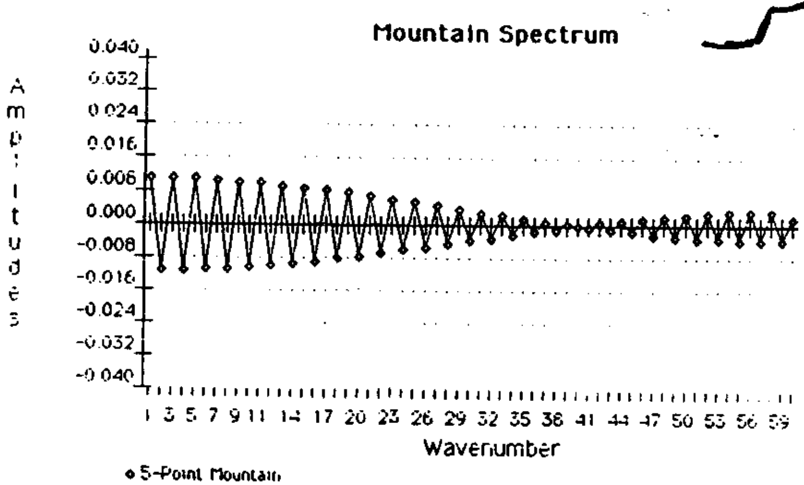

7-Point Mountain

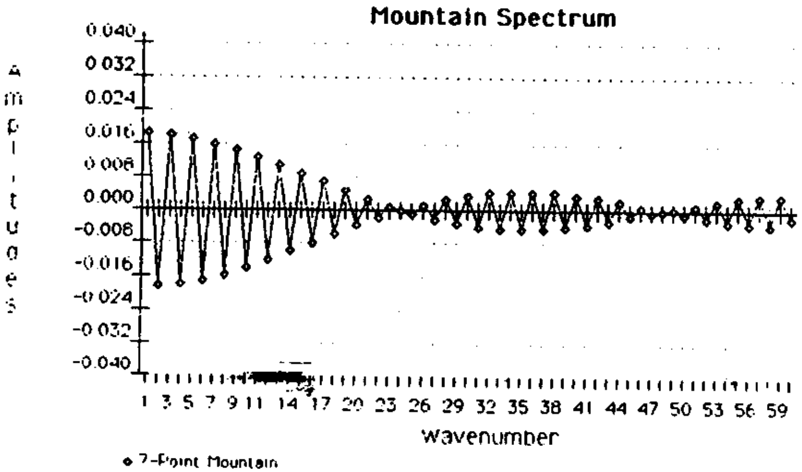

11-Point Mountain

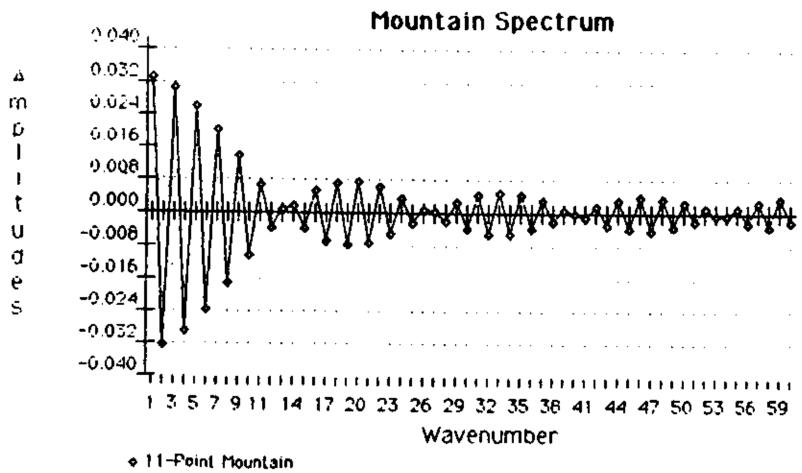

5-Point Mountain

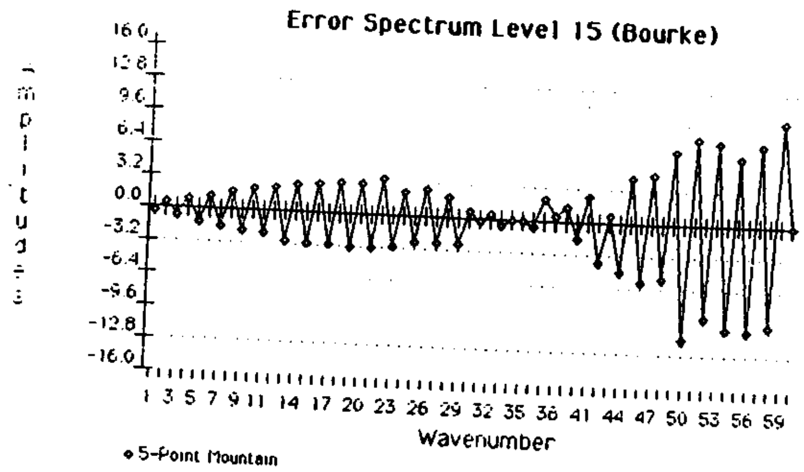

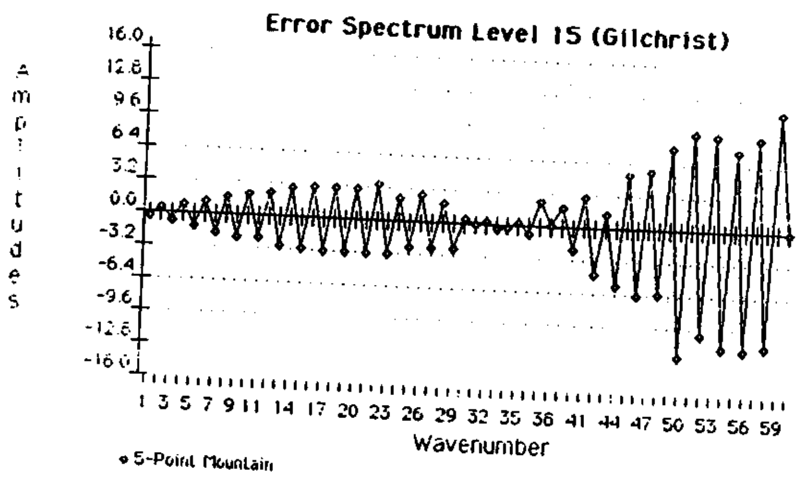

7-Point Mountains

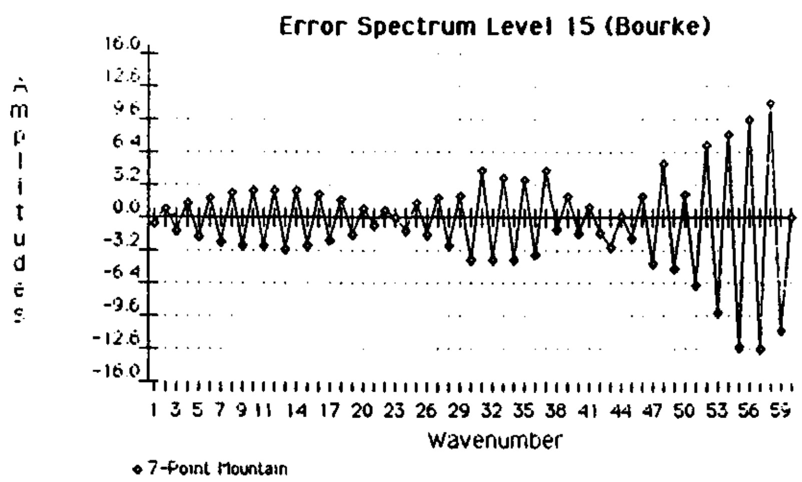

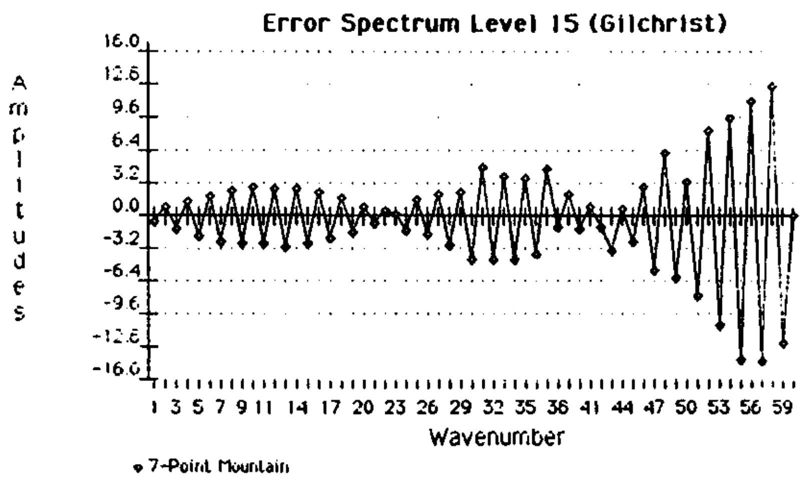

11-Point Mountains

Error Spectrum Level 15 (Bourke)

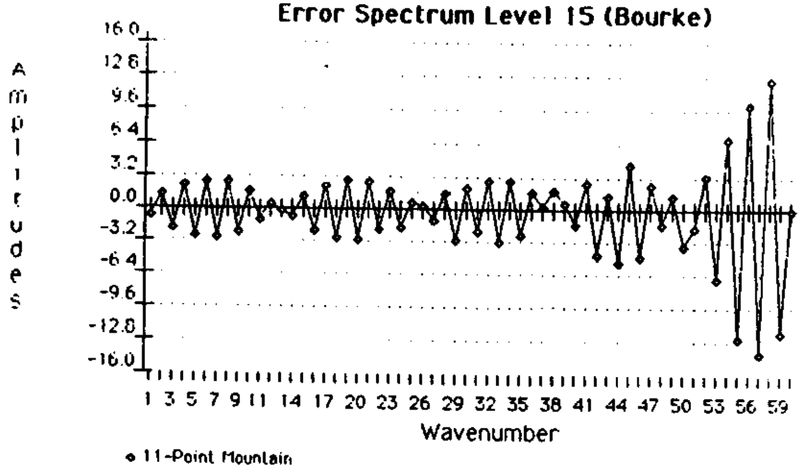

Error Spectrum Level 15 (Gilchrist)

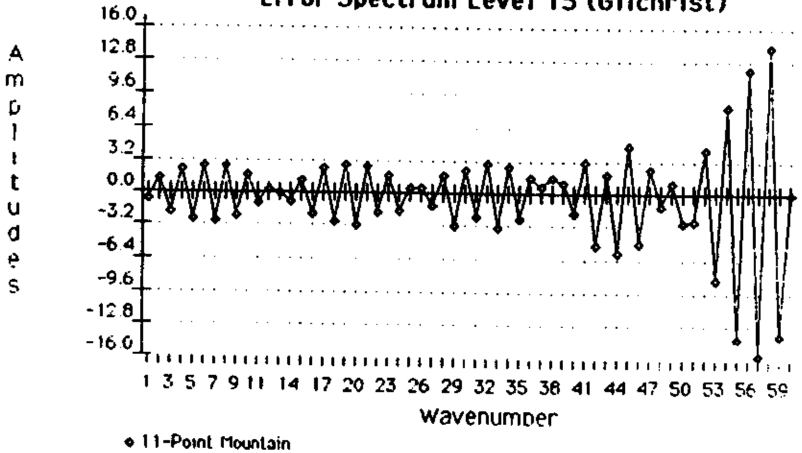

η - surfaces quasi-horizontal:

- no PGF error in the sense of σ syst
- no difficulties with [illegible] steep mountains etc.

*discontinuity: $p = p(z) \neq p_{rf}(z)$

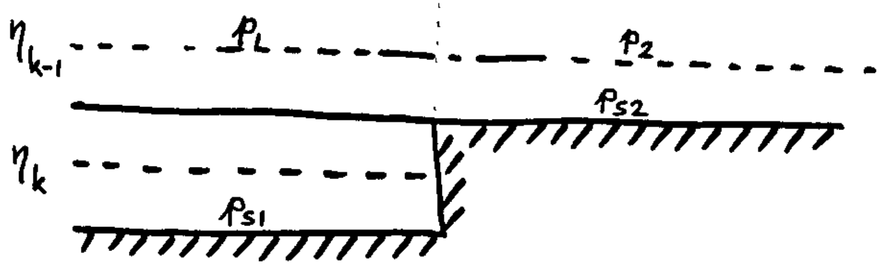

$$\eta_{k-1} = \frac{p_1 - p_T}{p_{S1} - p_T} \cdot \frac{p_{rf}(z_{S1}) - p_T}{p_{rf}(0) - p_T} = \frac{p_2 - p_T}{p_{S2} - p_T} \cdot \frac{p_{rf}(z_{S2}) - p_T}{p_{rf}(0) - p_T}$$

$$(p_1 - p_T) = (p_2 - p_T)\,\frac{p_{S1} - p_T}{p_{rf}(z_{S1}) - p_T} \cdot \frac{p_{rf}(z_{S2}) - p_T}{p_{S2} - p_T}$$

$p(z) \neq p_{rf}(z)$: [illegible]

[illegible]

- ✓ * internal boundaries } Mesinger et al. 1988
- ✓ * Vectorization
- ✓ * Physics

Janjić 1990

Pressure gradient force (PGF):
general form and physical meaning:

Janjić 1977, 80
Mesinger and Janjić 1985

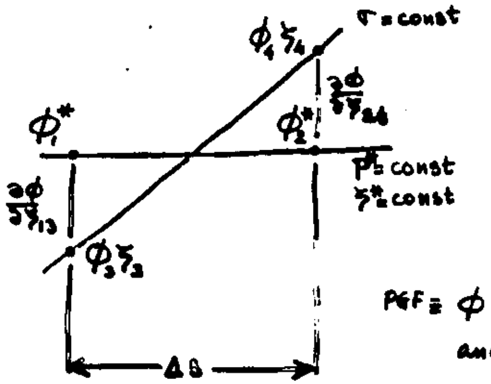

$$\Phi = \phi(x, y, \zeta)$$

$\zeta = \zeta(p)$,
Continuous,
monotonous

PGF = ϕ interpolated from σ to p* and differencing

$$\phi_1^* = \phi_3 + \frac{\partial\phi}{\partial\zeta_{13}}(\zeta^* - \zeta_3)$$

$$\phi_2^* = \phi_4 + \frac{\partial\phi}{\partial\zeta_{24}}(\zeta^* - \zeta_4)$$

$$-\frac{\phi_2^* - \phi_1^*}{\Delta s} = \frac{\phi_4 - \phi_3}{\Delta s} + \frac{1}{2}\left(\frac{\partial\phi}{\partial\zeta_{13}} + \frac{\partial\phi}{\partial\zeta_{24}}\right)\frac{\zeta_4 - \zeta_3}{\Delta s} - \frac{\frac{\partial\phi}{\partial\zeta_{24}} - \frac{\partial\phi}{\partial\zeta_{13}}}{\Delta s}\frac{1}{2}(2\zeta^* - \zeta_3 - \zeta_4)$$

$\Delta s \to 0$:

$$-\nabla_p \phi = -\nabla_\sigma \phi + \frac{\partial\phi}{\partial\zeta}\nabla_\sigma \zeta$$ – General form of PGF

Example: $\zeta = \ln p$:

$$-\nabla_p \phi = -\nabla_\sigma \phi - RT\,\nabla_\sigma \ln p.$$

Discretization of PGF

Usual vertical distribution of variables:

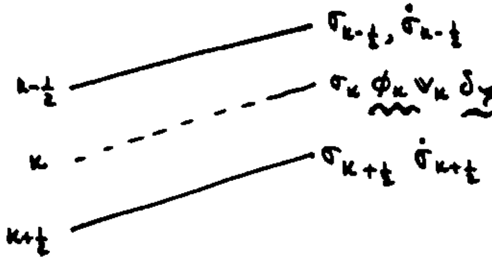

3 steps:
1. ϕ^k
2. ϕ^*
3. $\delta_x \phi^*$

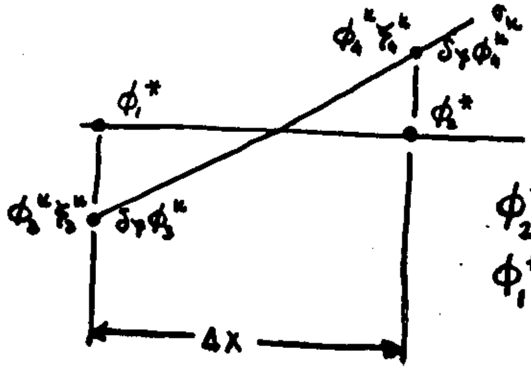

$$\phi_2^* = \phi_4^k + \delta_\zeta \phi_4^k(\zeta^* - \zeta_4^k)$$

$$\phi_1^* = \phi_3^k + \delta_\zeta \phi_3^k(\zeta^* - \zeta_3^k)$$

$$-\delta_x \phi^* = -\frac{\phi_2^* - \phi_1^*}{\Delta x} = -\frac{\phi_4^k - \phi_3^k}{\Delta x} + \frac{1}{2}(\delta_\zeta \phi_3^k + \delta_\zeta \phi_4^k)\frac{\zeta_4^k - \zeta_3^k}{\Delta x}$$

$$\zeta(p^*) = \zeta^* = \frac{1}{2}(\zeta_3^k + \zeta_4^k)$$

Hydrostatic inconsistency

Vd.14

(Rousseau and Pham ; Janjić)

$$\phi^{k+1} - \phi^{k} = \frac{1}{2}(\delta_{\gamma'}\phi^{k+1} + \delta_{\gamma'}\phi^{k})(\gamma'^{k+1} - \gamma'^{k})$$

γ' may not coincide with γ! (Arakawa, Arakawa and Mintz)

$\delta_{\gamma}\phi_{k}$ used for extrapolation from σ_{k} to γ^{*}

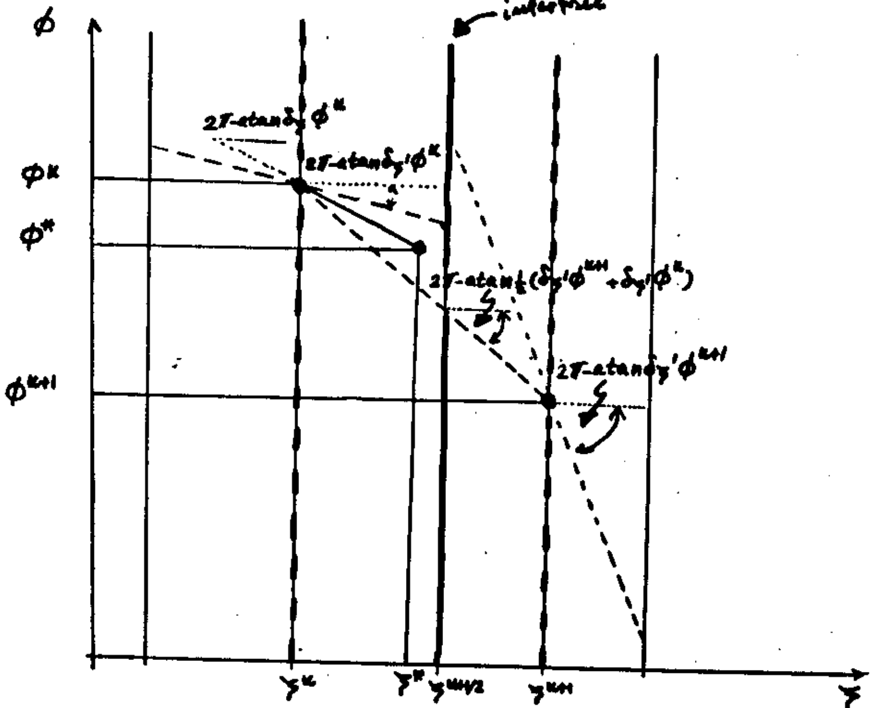

even if $\gamma = \gamma'$: (γ^{*}, ϕ^{*}) off the line connecting $(\gamma^{k+1}, \phi^{k+1})$ and (γ_{k}, ϕ^{k})

4. Hydrostatic consistency

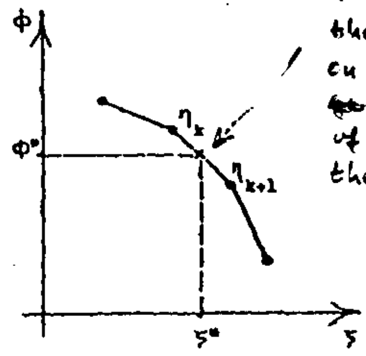

ϕ^{*} obtained in the 2nd step lies on the piecewise ~~[illegible]~~ linear profile of ϕ obtained in the first step

Fig. 6. Schematic representation of vertical profile of geopotential defined by the finite difference hydrostatic equation.

* hydrostatic consistency difficult to achive on "non-staggered" grids
  ex: Corby et al. scheme hydrostatically inconsistent (detailed analysis in the notes!)

* "staggered" grid natural for hydrostatic consistency

alternative: "staggered" distribution

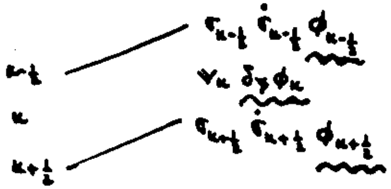

σ and γ defined at the interfaces only

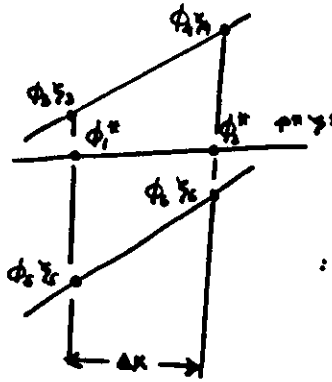

linear interpolation:

$$\phi_2^* = \phi_4 + \frac{\phi_6 - \phi_4}{\gamma_6 - \gamma_4}(\gamma^* - \gamma_4) = \overline{\phi}^\sigma + \delta_\gamma \phi (\gamma^* - \overline{\gamma}^\sigma)$$

def: $\overline{\phi}^\sigma = \frac{1}{2}(\phi_6 + \phi_4)$; $\delta_\gamma \phi = \frac{\phi_6 - \phi_4}{\gamma_6 - \gamma_4}$

$$-\delta_x \phi^* = -\delta_x \overline{\phi}^\sigma - \overline{\delta_\gamma \phi}^x \delta_x(\gamma^* - \overline{\gamma}^\sigma) - \overline{(\gamma^* - \overline{\gamma}^\sigma)}^x \delta_x(\delta_\gamma \phi)$$

$\gamma^* \equiv \overline{\overline{\gamma}^\sigma}^x$ (def. of height at which P.G.F. and consequently u is calculated)

$\Downarrow$

$$-\delta_x \phi = -\delta_x \overline{\phi}^\sigma + \overline{\delta_\gamma \phi}^x \delta_x \overline{\gamma}^\sigma$$

hydrostatically consistent

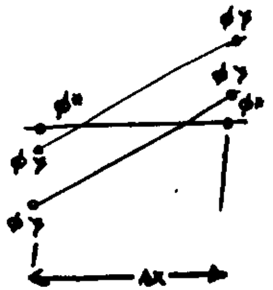

Example of hydrostatic inconsistency on staggered grid in the vertical; high vertical and inadequate horizontal resolution

$$|\delta_x \phi|_\sigma \Delta x \leqq |\delta_\sigma \phi| \Delta\sigma$$

R. HANEY:

Ocean σ model

disturbance amplitude of 3°C, Tables 1 and 2 indicate that the pressure gradient error in a 10-level model over the continental rise would be about 10 cm s^{-1} or 12 cm s^{-1}, depending on whether a reference state density profile is removed or not. The corresponding error in a 30-level model would be about an order of magnitude smaller.

As a final example of the kind of error that exists near steep topography in σ-coordinate models, we show the truncation error using a horizontal and vertical resolution that results in a hydrostatically inconsistent scheme. The results shown in Fig. 6, computed with $\delta x = 1$ km, are all based on a hydrostatically consistent scheme since (1) is satisfied for $K \leq 50$. To examine inconsistent schemes, we recomputed the largest truncation error in the water column, as in Fig. 6, but with different values of the grid size δx. Fig. 7 shows the results for $\delta x = 5$ and 10 km respectively. With $\delta x = 5$ km (Fig. 7a), the consistency requirement (1) is satisfied only for $K \leq 25$. Larger values of K result in sufficiently small $\delta\sigma$'s that (1) is violated. In this situation the scheme does not converge, and *increasing* the vertical resolution beyond K = 25 results in a *larger* truncation error, as pointed out by Janjic (1977) and Mesinger (1982). As predicted by (1), the situation is worse with $\delta x = 10$ km (Fig. 7b). In this case, the scheme is hydrostatically consistent only for $K \leq 12$. This example clearly shows the complex nature of the pressure gradient force error in σ-coordinate models. It is obviously essential to choose the horizontal and vertical resolution carefully, not only to accommodate the particular ocean problem at hand, but also to satisfy the hydrostatic consistency condition (1).

5 Summary and conclusions

This study analyses and documents the truncation error, and the error due to hydrostatic inconsistency, associated with computing the pressure gradient force over steep topography in σ-coordinate ocean models. The intent of the study is neither to advocate nor to discredit the use of σ-coordinates for studying flow over steep topography. The purpose is simply to document the errors associated with given profiles of buoyancy and pressure typical of synoptic disturbances in the ocean. A major objective is to investigate how the errors depend on the model parameters, primarily resolution, and the vertical structure of the di...

6. The error problem: a numerical example

Atmosphere in hydrostatic equilibrium: PGF ≟ 0

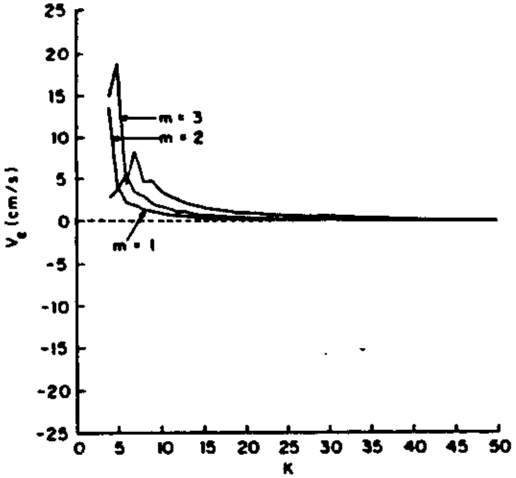

← 6

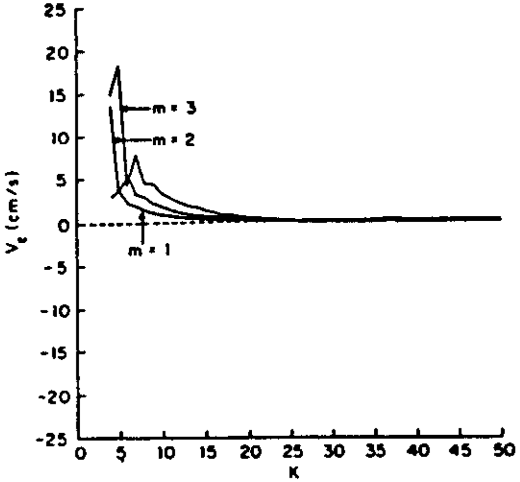

↖a
7
↙b

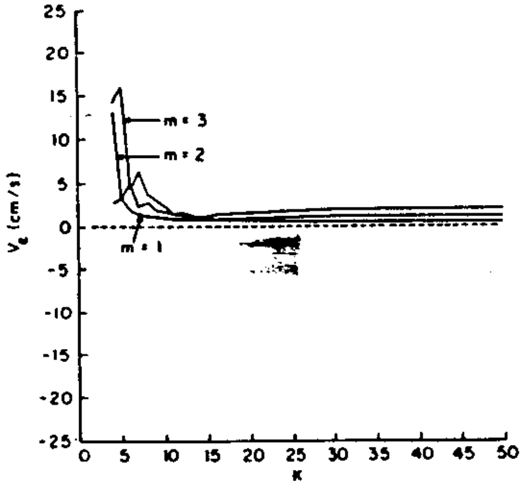

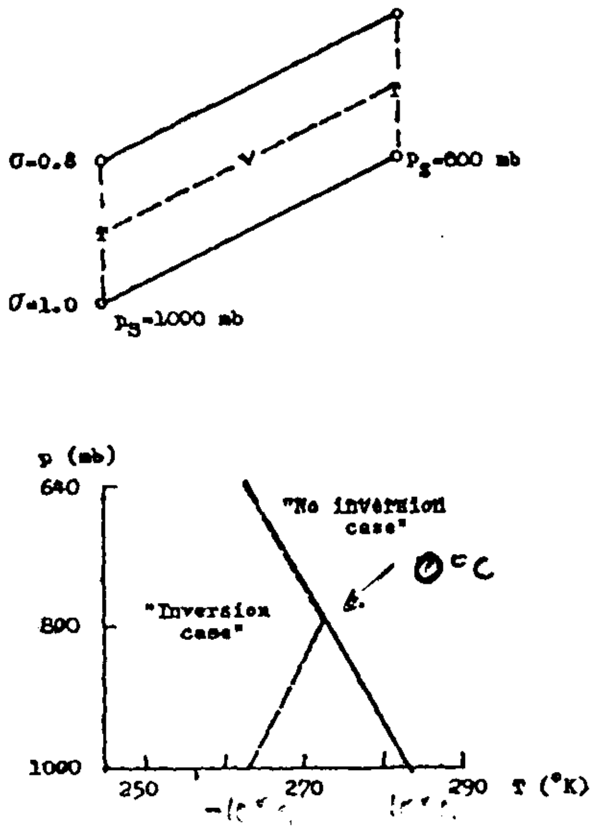

Fig. 11. The temperature profiles used to calculate the errors of the Corby et al. and of Burridge and Haseler pressure gradient force scheme (lower panel), and the location of the grid point at which the errors were calculated (upper panel). (After Mesinger, 1982)

Mesinger 1982

Table 1.

Errors of the pressure gradient force analogs obtained using the Corby et al. and the Burridge and Haseler scheme, for the "no inversion case" and the "inversion case"; see text for details. Values are given in increments of geopotential ($m^2 s^{-2}$), between two neighboring grid points, along the direction of the increasing terrain elevations. (Note that some of the numbers in the last two lines are slightly different from those published in the referred paper; this is a result of the removal of an error that Mesinger has found in his program for calculation of the Burridge and Haseler scheme values. The numbers published previously actually represented errors of a scheme which within the geopotential gradient term used geopotentials of the $\sigma = 0.9$ surface, rather than values defined by (4.22).)

	$\Delta\sigma$ = 1/5	1/15	1/25	...	lim $\Delta\sigma \to 0$
Corby et al. scheme "no inversion case"	151.2	-48.7	29.0	...	0
Corby et al. scheme "inversion case"	-159.6	-159.6	-159.6	...	-159.6
Burridge and Haseler scheme "no inversion case"	0	0	0	...	0
Burridge and Haseler scheme "inversion case"	0	-142.1	-153.3	...	-159.6

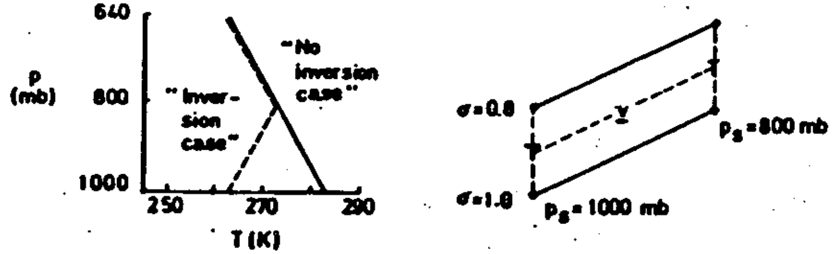

Fig. 1. The temperature profiles and the location of the grid point at which pressure gradient force errors were calculated by Mesinger (1982).

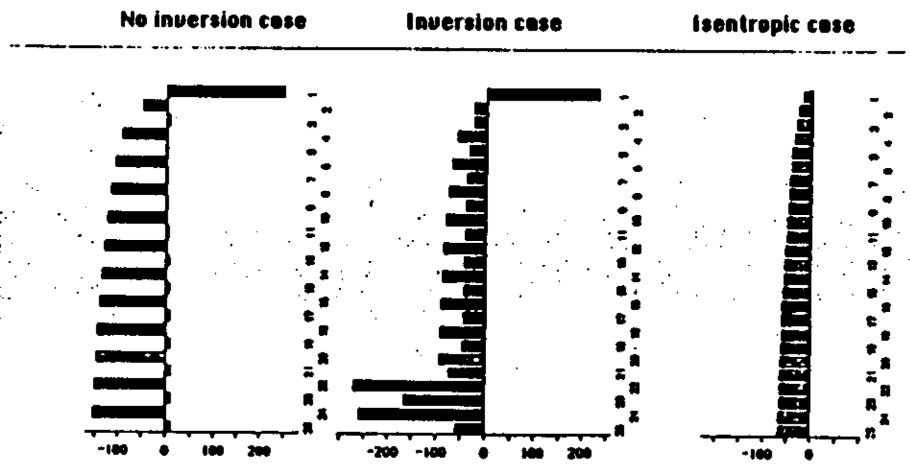

Fig. 2. Errors of the Arakawa (1972)-Brown (1974) pressure gradient force scheme, for the "no inversion case" (left hand panel), "inversion case" (middle panel) and an isentropic atmosphere (right hand panel), for a vertical structure of 25 sigma layers of equal thickness. Values are given in increments of geopotential ($m^2 s^{-2}$), between two neighboring grid points, along the direction of the increasing terrain elevations.

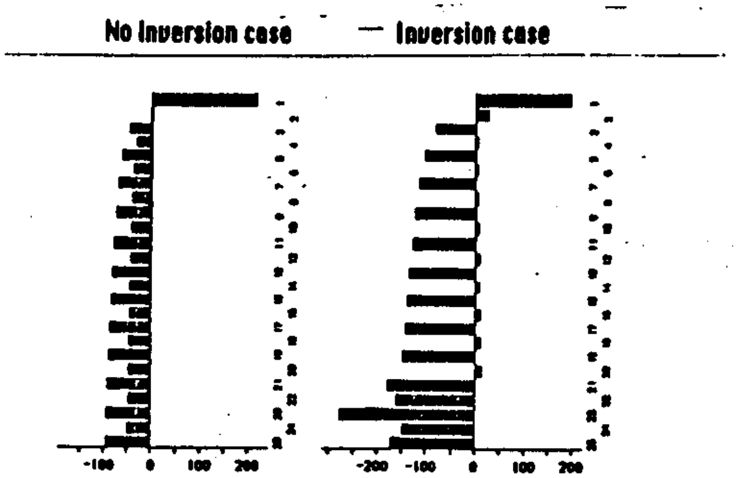

Fig. 3. Errors of the Nested Grid Model (see text for details) pressure gradient force scheme, for the "no inversion case" (left hand panel), and the "inversion case" (right hand panel), for a vertical structure of 25 sigma layers of equal thickness. Values are given in increments of geopotential ($m^2 s^{-2}$), between two neighboring grid points, along the direction of the increasing terrain elevations.

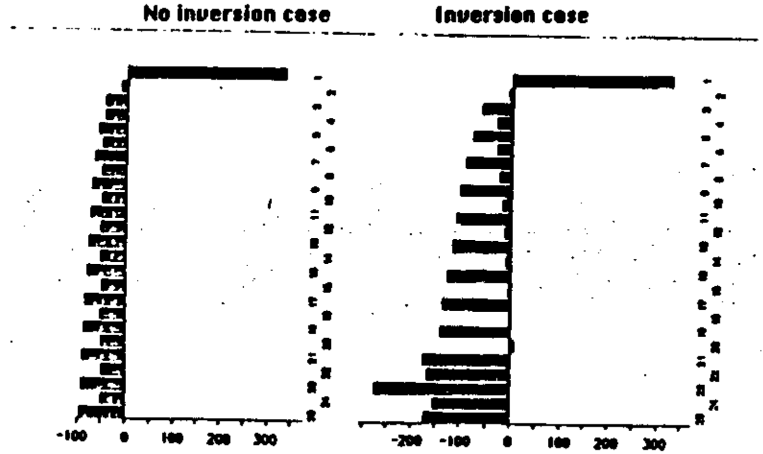

Fig. 4. Errors of the Arakawa-Suarez θ-conserving pressure gradient force scheme, expanded to include horizontal differencing, for the "no inversion case" (left hand panel), and the "inversion case" (right hand panel), for a vertical structure of 25 sigma layers of equal thickness. Values are given in increments of geopotential ($m^2 s^{-2}$), between two neighboring grid points, along the direction of the increasing terrain elevations.

v.d.19 6

PGF error in σ system:

Two sources of errors when calculating ϕ^* at z^* :

1. Integrating FD hydrostatic equation to calculate $\phi_{k+\frac{1}{2}}$ at $\sigma_{k+\frac{1}{2}}$ (not peculiar to σ system), centred – higher accuracy

2. Linear interpolation from $\sigma_{k\pm\frac{1}{2}}$ to z^* to calculate ϕ^* (peculiar to σ system), uncentred

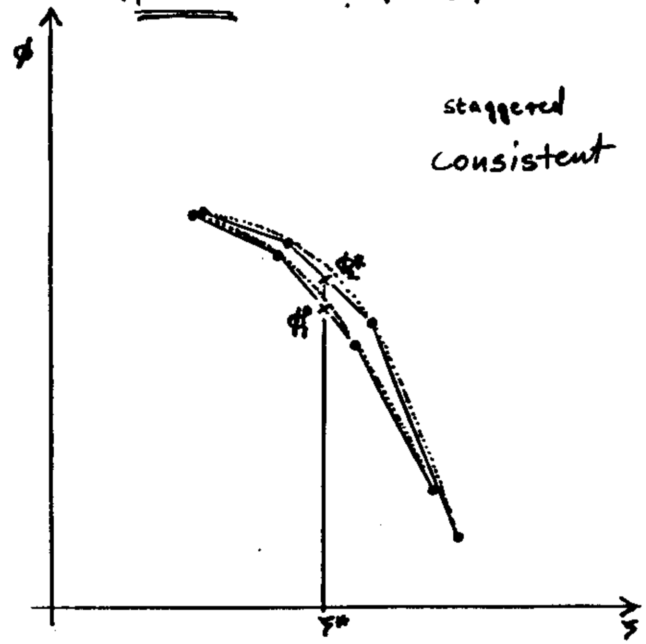

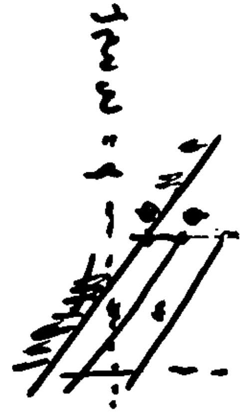

The situation essentially the same for non-staggered grid

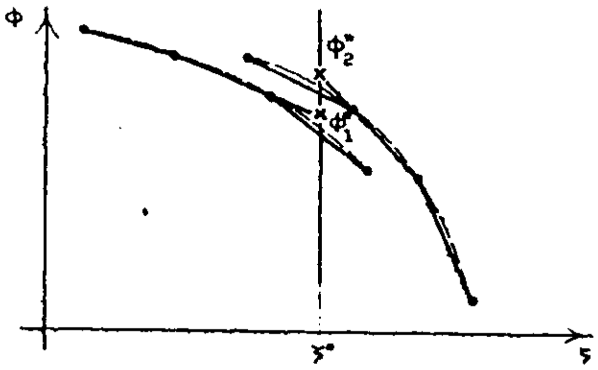

Fig. 13. Same as in Fig. 12, but for the case of hydrostatic inconsistency.

PGF error in the case of hydrostatic inconsistency, staggered

v.d.20

Minimization of interpolation error: Janjić 77, 80

$\phi = \text{const} \times \zeta \Rightarrow$ error-free linear interpolation !

Minimize the vertical variation of $\frac{\partial \phi}{\partial \zeta}$

(ϕ at interfaces calculated more accurately as well!)

Minimization of vertical variation of $\frac{\partial \phi}{\partial \zeta}$ by suitable choice

$$\frac{\partial \phi}{\partial p} = -\frac{RT}{p}$$

$$\frac{\partial \phi}{\partial \zeta} = -\frac{RT}{p\frac{d\zeta}{dp}}$$

No variation if $\frac{\partial^2 \phi}{\partial \zeta^2} = 0 \Rightarrow$

$$p\frac{d\zeta}{dp} = CT, \quad c = \text{const}$$

↳ Solution: Optimum ζ for any T profile

Optimum ζ for a set of temperature profiles,

e.g.

$$\min \left(\int \left(\frac{\partial^2 \phi}{\partial \zeta^2} \right)^2 \right)$$

Example:

$\xi = x^{1+m}$, $x = \ln p$

$$\frac{\partial \phi}{\partial \xi} = - \frac{R}{1+m} \frac{T}{X^{m}}$$

$$\int_{x_t}^{x_s} \frac{\partial}{\partial m} \frac{\partial^2 \phi}{\partial \xi^2} dx = 0. \Rightarrow 1 < m < 2, \; p_t = 200 \text{ mb}$$

p_t decreasing ⇒ m decreasing

HIBO, GFDL, ... :

$m = 1$ (compromise):

$$\delta_\xi \phi_k = - R \frac{T_k}{2 \ln p_k}, \quad \ln p_k = \frac{1}{2} (\ln p_{k-1/2} + \ln p_{k+1/2})$$

Phillips' test

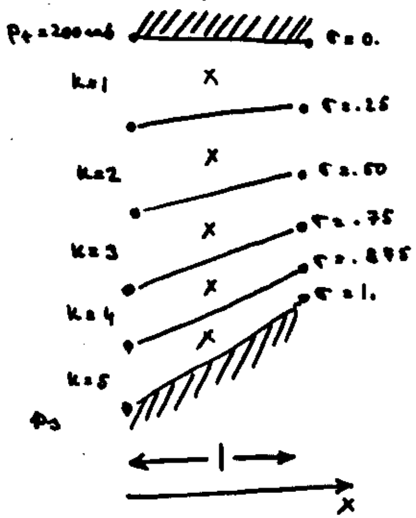

$\phi = 1054.5 + 80387.3 \, z - 768.0 \, z^2 + 810.0 \, z^3$

$z = -x + 4.51292546$

5-level HIBO resolution

$\sigma = \frac{p - p_t}{\pi}$, $\pi = p_s - p_t$

— ECMWF

— HIBV

— Minimum errors $\ln p^{1+m}$

m		k = 1	k = 2	k = 3	k = 4	k = 5
0.0	term I	4577.6	11177	14464	16221	17142
	term II	− 4423.7	11120	− 14439	− 16222	− 17144
	error	153.95	56.852	25.066	− 0.5508	− 2.6641
0.2	term I	4577.6	11177	14464	16221	17142
	term II	− 4450.2	− 11125	− 14441	− 16221	− 17144
	error	127.43	51.590	23.250	0.0391	− 2.0391
0.4	term I	4577.6	11177	14464	16221	17142
	term II	− 4477.4	− 11131	− 14443	− 16221	− 17144
	error	100.25	45.477	21.086	0.1484	− 1.0711
0.6	term I	4577.6	11177	14464	16221	17142
	term II	− 4504.5	− 11138	− 14445	− 16222	− 17143
	error	73.141	39.383	19.504	− 0.5234	− 1.3359
0.8	term I	4577.6	11177	14464	16221	17142
	term II	− 4531.6	− 11144	− 14448	− 16221	− 17144
	error	46.012	33.141	16.688	0.1172	− 2.2969
1.0	term I	4577.6	11177	14464	16221	17142
	term II	− 4559.1	− 11150	− 14450	− 16222	− 17144
	error	18.543	26.773	14.633	− 0.4258	− 1.9531
1.2	term I	4577.6	11177	14464	16221	17142
	term II	− 4586.4	− 11156	− 14453	− 16222	− 17144
	error	− 8.7891	20.484	11.859	− 0.5859	− 2.5781
1.4	term I	4577.6	11177	14464	16221	17142
	term II	− 4614.2	− 11163	− 14455	− 16222	− 17144
	error	− 36.559	13.828	9.4219	− 1.0859	− 2.2930
1.6	term I	4577.6	11177	14464	16221	17142
	term II	− 4641.8	− 11170	− 14458	− 16223	− 17144
	error	− 64.100	7.2659	6.9141	− 2.0859	− 2.2188
1.8	term I	4577.6	11177	14464	16221	17142
	term II	− 4669.5	− 11177	− 14461	− 16223	− 17145
	error	− 91.863	0.3672	3.7109	− 1.9258	− 3.5938
2.0	term I	4577.6	11177	14464	16221	17142
	term II	− 4697.4	− 11183	− 14464	− 16224	− 17146
	error	− 119.82	− 6.5391	0.9023	− 2.9336	− 3.8047

Table 1. The first and the second term of the pressure gradient force approximation as well as their sum as a function of parameter m. All values are given in m^2/sec^2.

Higher order (2nd) interpolation helpful (Mihailović + Janjić 1986)

5-Point Mountain

RMS Error (Bourke)

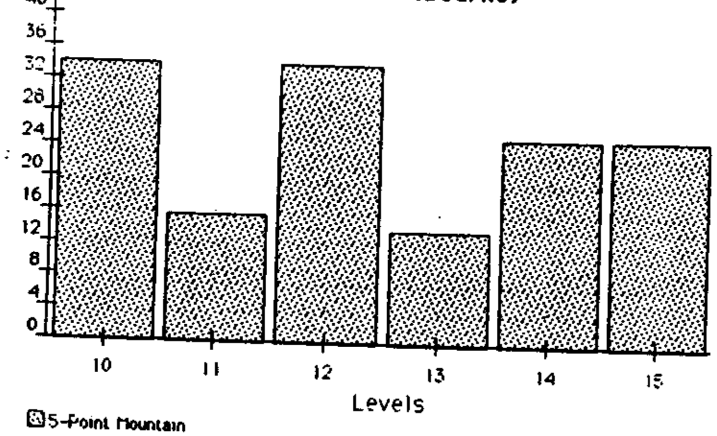

RMS Error (Gilchrist)

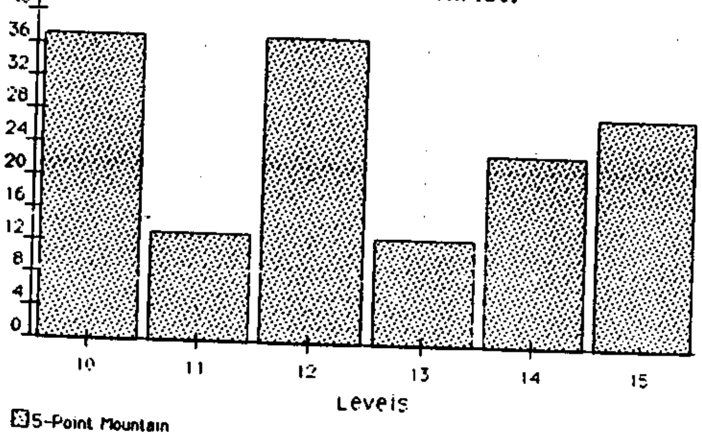

7-Point Mountain

RMS Error (Bourke)

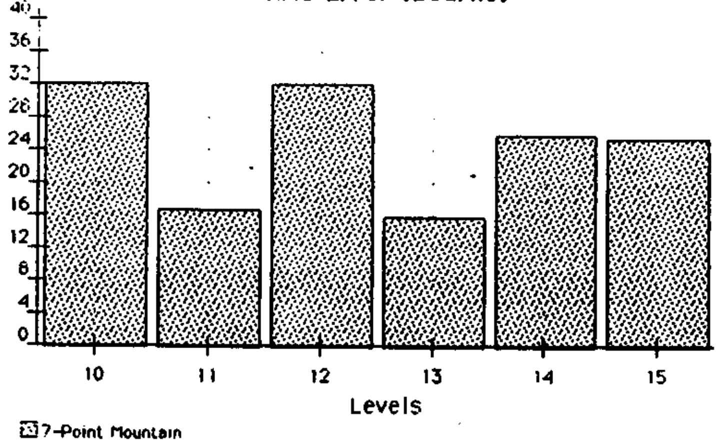

RMS Error (Gilchrist)

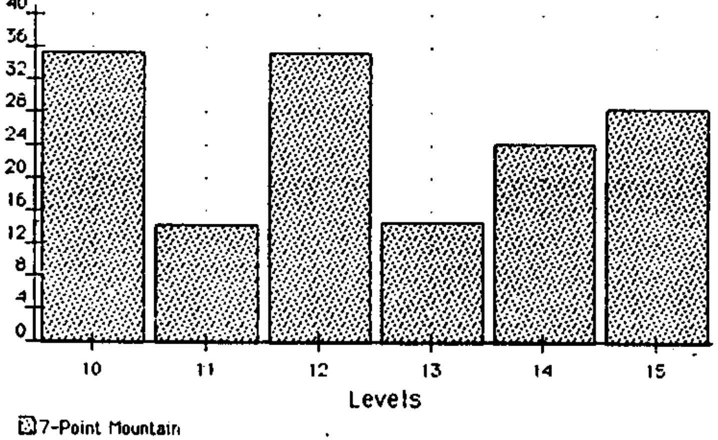

11-Point Mountain